Analysis of Mass Flows and Membrane Crossover in CO2 Reduction at High Current Densities in a MEA-Type Electrolyzer

Larrazábal, Gastón O; Strøm-Hansen, Patrick; Heli, Jens P.; Zeiter, Kevin; Therkildsen, Kasper T.; Chorkendorff, Ib; Seger, Brian

Published in:
ACS Applied Materials and Interfaces

Link to article, DOI:
10.1021/acsami.9b13081

Publication date:
2019

Document Version
Peer reviewed version

Energy, Environmental, and Catalysis Applications

Analysis of Mass Flows and Membrane Crossover in CO2 Reduction at High Current Densities in a MEA-Type Electrolyzer

Gastón O. Larrazábal, Patrick Strøm-Hansen, Jens P. Heli, Kevin Zeiter, Kasper T. Therkildsen, Ib Chorkendorff, and Brian Seger

ACS Appl. Mater. Interfaces, **Just Accepted Manuscript** • DOI: 10.1021/acsami.9b13081 • Publication Date (Web): 11 Oct 2019

Analysis of Mass Flows and Membrane Crossover in CO_2 Reduction at High Current Densities in a MEA-Type Electrolyzer

Gastón O. Larrazábal,[1] Patrick Strøm-Hansen,[1] Jens P. Heli,[1] Kevin Zeiter,[2] Kasper T. Therkildsen,[3] Ib Chorkendorff,[1] and Brian Seger[1,]*

[1] Surface Physics and Catalysis (SurfCat) section, Department of Physics, Technical University of Denmark, 2800 Kgs. Lyngby, Denmark

[2] Institute for Chemical and Bioengineering, Department of Chemistry and Applied Biosciences, ETH Zurich, 8093 Zurich, Switzerland

[3] Siemens A/S, 2800 Kgs. Lyngby, Denmark

KEYWORDS: electrocatalysis, CO_2 reduction, silver, anion-exchange membrane, membrane-electrode assembly, electrolyzer

ABSTRACT

Cell designs that integrate membrane-electrode assemblies (MEAs) with highly selective catalysts are a promising route to reduce ohmic losses and achieve high energy efficiency in CO_2 reduction at industrially relevant current densities. In this work, porous silver filtration membranes are demonstrated as simple and efficient gas-diffusion electrodes for CO_2 reduction to CO at high current densities in a MEA-type device. A partial current density for CO of up to ca. 200 mA cm^{-2} was achieved at a cell voltage of ca. 3.3 V, in tandem with minimal H_2 production. However, the analysis of cathodic and anodic outlet streams revealed that CO_2 crossover across the AEM, mostly in the form of CO_3^{2-} but partially as $HCOO^-$ generated over the cathode, actually exceeds the amount of CO_2 converted to the target product, resulting in a poor utilization of the reactant and in the early onset of mass transfer limitations. In addition, CO_2 crossover leads to non-stoichiometric decrease of the outlet flow rate from the cathodic compartment that can lead to a substantial overestimation of catalytic performance if the inlet flow rate of CO_2 is used as reference for calculating partial current densities and Faradaic efficiencies. The results of this work highlight the importance of carrying out a carbon balance, in addition to traditional measurements of activity and selectivity, to adequately assess the performance of CO_2 reduction devices at high current densities, and inform future efforts aimed at mitigating membrane crossover in MEA-type electrolyzers for CO_2 reduction.

1. INTRODUCTION

Combining the electrochemical CO_2 reduction reaction (eCO_2RR) with carbon-neutral energy sources offers exciting perspectives for using CO_2 as a sustainable feedstock for the production of fuels and chemicals.[1–3] Research efforts over recent years have led to a substantial expansion of the fundamental understanding of CO_2 electroreduction[4–6] and, in particular, to the discovery of catalyst compositions and morphologies that show high performance (i.e., low overpotentials and high Faradaic efficiencies) toward CO and $HCOO^-$, the simplest eCO_2RR products.[7] However, recent technoeconomic analyses have emphasized the importance of achieving high current densities (i.e., hundreds of $mA\,cm^{-2}$) in relation to the practical viability of the eCO_2RR,[8,9] which demands the adoption of gas diffusion electrodes (GDEs) that allow high local concentrations of CO_2 and support much higher reaction rates than planar electrodes in aqueous electrolytes.[10] In this context, there is a growing awareness of the need to evaluate eCO_2RR catalysts under realistic operating conditions,[11] and to investigate the link between different cell configurations and electrocatalytic performance to derive design guidelines for CO_2 reduction devices.

Due to its high selectivity and moderate cost, silver shows interesting properties as a practical catalyst for CO_2 reduction to CO.[12–14] Bidault and Kucernak investigated the use of porous Ag membranes, commonly used as filtration media in biotechnological applications, as cathodic GDEs in alkaline fuel cells.[15] In contrast to traditional carbon-based GDEs, these porous membranes integrate electrocatalytic functionality, mechanical support, and efficient current conduction (due to the very high electrical conductivity of Ag) within a single, homogeneous structure. Porous Ag membranes have a comparable cost to carbon gas diffusion layers (GDLs),[16] and they might overcome some of the drawbacks associated to the latter, such as the

gradual loss of hydrophobicity[17] and accelerated degradation under alkaline conditions.[18] Consequently, we sought to assess the potential of commercially available porous Ag membranes as GDEs for CO_2 reduction at high current densities.

Besides having a catalyst that is highly active and selective, achieving high energy efficiency at elevated current densities requires optimizing the design of the electrolyzer to attain low ohmic losses.[19] Recent studies have demonstrated the use of highly alkaline catholytes in contact with the GDE to manipulate the reaction environment and achieve high electrocatalytic performance.[17,20,21] However, the practicality of such cell designs is likely limited by the penetration of CO_2 into the catholyte layer and by high ohmic losses arising from the poor conductivity of liquid electrolyte solutions.[11] By greatly reducing the distance between the electrodes and eliminating the need of a liquid electrolyte, membrane electrode assemblies (MEAs) can decrease significantly the cell ohmic overpotential.[10,22] It is known that cation-exchange membrane-based MEAs show poor results in CO_2 reduction because they generate a highly acidic reaction environment that heavily favors the competing hydrogen evolution reaction (HER).[23,24] This fact has led to the exploration of cell designs employing bipolar (BPM) or anion-exchange membranes (AEM). BPM-based configurations have showed encouraging results but have also exposed the difficulty of effectively suppressing the HER as well as stability concerns related to the delamination of the acidic and alkaline layers.[25–27] In contrast, AEM-based devices have exhibited outstanding selectivity and stability at high current densities, particularly in CO_2 reduction to CO.[28–30] Nevertheless, CO_2 crossover from the cathodic to the anodic compartment of the cell, caused by the neutralization of CO_2 to HCO_3^-/CO_3^{2-} and the transport of these anionic species across the membrane, has been recognized as a significant limitation of AEM-based devices.[27,30] This phenomenon has been reported in several CO_2

reduction studies in high-current electrolyzers (usually at a single operating point),[27,28,31,32] and Xiang et al. recently carried out a study of the impact of crossover on CO_2 utilization in an aqueous (i.e., H-type) cell using different types of ion-selective membranes.[33] Nevertheless, there is currently a lack of systematic analyses of CO_2 crossover at industrially relevant current densities using a zero-gap configuration.[31] In this context, we herein present a full mass balance—anchored in the analysis of both cathodic and anodic outlet streams—that provides a comprehensive picture of CO_2 crossover in MEA-type electrolyzers, with the aim of informing future efforts geared toward the optimization of this promising class of CO_2 reduction devices.

2. EXPERIMENTAL

2.1. Cell configuration. This work was conducted using a commercially available electrolyzer (Liquid-Gas Fuel Cell Test Fixture, Scribner Associates) equipped with gold-plated copper current collectors and graphite and titanium serpentine flow fields for the cathode and anode, respectively (**Figure 1A**). Porous silver membranes with a nominal pore size of 1.2 μm (Sterlitech Inc., purity 99.97%, area 4 cm^2) were used as cathodes. Commercially available IrO_2-coated carbon paper electrodes (Dioxide Materials, area 7.3 cm^2), previously described by Kutz et al.[28] were employed as anodes. A fresh membrane-electrode assembly was constructed for each experiment by intercalating a fresh Sustainion X37-50 grade 60 anion-exchange membrane (Dioxide Materials, 16 cm^2) between the electrodes and fastening the bolts of the cell with a torque of 4 N m. Each electrode was surrounded by PTFE gaskets for protection and electrical insulation. The cathodic flow field was fed with CO_2 (AGA, purity 4.5) at a flowrate of 100 $ml_n\ min^{-1}$, which was humidified upstream of the cell by sparging into a container filled with ultrapure water. Reference conditions for the gas flows in this work are defined as 273.15 K

and 1 bar ($1\ ml_n\ min^{-1} = 7.434 \times 10^{-7}\ mol\ s^{-1}$). The anodic flow field was fed with a 0.1 M $KHCO_3$ solution (Sigma-Aldrich, 99.995% trace metal basis) which was recirculated continuously at a flowrate of 60 $cm^3\ min^{-1}$ using a diaphragm pump. The device was heated using two cartridge heaters inserted into each end plate and connected to an external temperature controller, with feedback from a thermocouple inserted into the cathodic end plate.

2.2. Characterization and electrochemical tests. Given the large currents involved, the electrolyses were carried out in galvanostatic mode (range: 200-1600 mA, step size: 200 mA) using a direct current (DC) power supply (Aim-TTi CPX400DP) connected to the current collectors of the cell. The cell voltage was measured continuously with a 16-bit analog-to-digital converter (Microchip Technology MCP3428) interfaced with a Raspberry Pi. A solenoid valve (SMC Instruments, VQD1151 series) was installed upstream of the cell to switch between sampling and venting the outlet streams from each compartment (**Figure 1B**). A homemade Python program controlled the setup and recorded the data at regular intervals. The accuracy of the cell voltage measurements under operating conditions was validated with a Bio-Logic VSP-300 potentiostat with no current passing through the instrument, with the working and reference electrode terminals connected to the cathodic and anodic current collectors, respectively.

Scanning electron microscopy (SEM) imaging of the porous Ag electrodes at an accelerating voltage of 15 kV was performed in a FEI Quanta 200 FEG instrument operating in secondary electron mode. X-ray photoelectron spectroscopy (XPS) analysis was carried out with monochromated Al Kα radiation (1486.7 eV) in a ThetaProbe instrument (Thermo Fisher Scientific) equipped with a hemispherical analyzer. Survey scans were acquired in the binding energy range of 0-1400 eV with an analyzer pass energy of 100 eV.

2.3. Flow measurement and product analysis. The molar flow rate of the cathodic and anodic outlet streams of the electrolyzer was measured continuously with either a volumetric flow meter (MesaLabs, Defender 530+) or a mass flow meter (MFM) placed upstream of the gas chromatograph (GC), as shown in **Figure 1B**. For the MFM, a multivariable calibration procedure was carried out to convert the composition-dependent signal of the instrument into the actual molar flow rate and validated with a primary flow calibrator (details provided in the Supporting Information). The composition of the gas streams was determined with a PerkinElmer Clarus 580 instrument equipped with Molecular Sieve 13X and HayeSep Q packed columns, operating with argon as carrier gas at a flow rate of 15 ml min^{-1}. H_2, CO_2 and O_2 were quantified with the thermal conductivity detector (TCD) while CO was passed through a methanizer and quantified with the flame ionization detector (FID). GC runs were initiated every 30 min. Post-reaction high performance liquid chromatography (HPLC) analysis of the anolyte was carried out in an Agilent 1200 series system equipped with a Bio-Rad Aminex HPX-87H column heated to 50 °C and refractive index (RID) and diode array (DAD) detectors. An aqueous solution of H_2SO_4 (5 mM, flowing at 0.6 ml min^{-1}) served as the eluent. Additional details on the calculation of the partial current densities and Faradaic efficiencies for each product are provided in the Supporting Information.

3. RESULTS AND DISCUSSION

3.1. Electrode characterization and cell design. Commercially available porous Ag membranes provide an interesting platform to develop carbon-free gas diffusion electrodes for CO_2 reduction electrolyzers. In this work, we used membranes with a nominal pore size diameter of 1.2 μm and a thickness of 50 μm,[34] although inspection by scanning electron microscopy

(SEM) revealed that the surface of the Ag membranes is populated by well-connected pore openings of considerably larger size (2-5 μm, **Figure 1A**). The area-based density of the material is ca. 27 mg cm^{-2}, implying a porosity of ca. 55%. Post-reaction SEM analysis showed no changes to the porous structure of the electrode, evidencing its stability during CO_2 reduction at high current densities. The stated purity of the Ag membranes (Sterlitech Corporation) is 99.97%. The XPS survey scan of the Ag membranes revealed the presence of adventitious carbon and oxygen, as well as minor peaks that indicated the presence of chlorine, possibly due to the formation of AgCl during production or handling (**Figure S1**). Nevertheless, no metallic impurities that might interfere with the eCO_2RR were observed within the limit of detection of the XPS analysis.

We prepared each MEA by intercalating a Sustainion anion-exchange membrane between the porous Ag cathode ($A_{cathode}$ = 4 cm^2) and an IrO_2/C anode (Dioxide Materials). The cathode was fed with humidified CO_2, while the anode was fed with a 0.1 M $KHCO_3$ solution, which was freshly prepared at the beginning of each test, but recycled during the duration of the test. This "exchange-MEA" configuration (i.e., vapor-fed cathode and liquid-fed anode) is expected to afford lower ohmic losses compared to cell designs employing liquid catholyte layers, while avoiding problems due to poor membrane hydration at high current densities with fully gas-fed electrolyzers (i.e., a "full-MEA" configuration).[22] The outlet streams both from the cathode and the anode were analyzed by GC and the corresponding molar flow rates were measured with a mass flow meter installed between the outlet of the cell and the gas chromatograph (**Figure 1B**). As will be shown in the following discussion, measuring the non-stoichiometric loss of CO_2 to the anodic compartment is necessary to assess accurately the performance of CO_2 reduction devices at high current densities.

3.2. Electrochemical performance. Figure 2 shows the typical performance of the electrolyzer toward the main products (CO and H_2) and the overall cell voltage as a function of the total current density. The experiments were carried out in galvanostatic mode by stepping (at 1 hour intervals) successively the total current density from 50 to 400 mA cm^{-2}. The device was held at 30 °C to maintain a constant temperature throughout testing. The cell voltage was recorded continuously and the gas products were analyzed periodically by gas chromatography (GC). When argon instead of CO_2 was fed into the electrolyzer, H_2 was the only product formed over the cathode with a Faradaic efficiency of 100% at all current densities (**Figure S2**), excluding the existence of short circuits within the cell (which would lead to a large non-redox current and thus to a FE_{H2} much lower than 100%) as well as any eCO_2RR activity arising from diffusion of the bicarbonate electrolyte from the anode to the cathode.

The production of CO over porous Ag electrodes in the MEA-type electrolyzer reached a maximum rate of ca. 200 mA cm^{-2} (3.74 mmol h^{-1} cm^{-2}) at a cell voltage of 3.3 V. Up to a total current density of 250 mA cm^{-2}, the HER was negligible and CO was almost exclusively produced in the gas phase (**Figure 2B**). This increase in current without an increase in CO or H_2 (or any other gas) production clearly indicates that liquid products must be formed. However, increasing the total current density beyond 250 mA cm^{-2} resulted in the light-off of hydrogen evolution accompanied with periodic oscillations of the cell voltage (and conversely, with oscillations of the current when a constant cell voltage was imposed) associated to the appearance of mass transfer limitations (**Figure S3**). These mass transfer limitations are likely a result of flooding of the cathode because of water migration, as predicted by Weber et al. for a MEA-type setup with a liquid-fed anode.[22] We remark that we did not observe salt precipitation

at the cathode, although current densities were below the value at which the solubility limit of K_2CO_3 is predicted to be reached (ca. 750 mA cm^{-2}).[22]

Overall, the results in **Figure 2** underscore the effectiveness of a MEA approach with an anion-exchange membrane to achieve high rates for CO_2 reduction to CO and highlight the potential of the Ag filtration membranes as simple and robust cathodes for CO_2 reduction.

As previously eluded to, at current densities of 250 mA cm^{-2} and above, the sum of the Faradaic efficiencies (FEs) for CO and H_2 was significantly lower than 100% (**Figure 2C**). Besides CO and H_2 in the gas phase, $HCOO^-$ was detected after the reaction by high-performance liquid chromatography (HPLC) both in the anolyte and in droplets condensed from the cathodic compartment of the cell (**Table S1**). Consequently, the Faradaic efficiency that is not accounted for by the gas-phase products (labeled as "Others" in **Figure 2C**) can be reasonably attributed to CO_2 reduction to $HCOO^-$ over the cathode and to its oxidation over the anode (calculation details are provided in the Supporting Information). These results indicate that CO_2 reduction to $HCOO^-$ is a significant side reaction over the porous Ag electrodes in a MEA-type configuration. Previous studies in H-type cells have shown that $HCOO^-$ is a minor eCO_2RR product at highly cathodic potentials over poly-[13,35] and single-crystalline[36,37] Ag electrodes, although in most reports Faradaic efficiencies for this product do not typically exceed 10%. Nevertheless, there has been one report that suggests this fraction may be significantly higher at potentials more cathodic than −1.3 V vs. RHE.[37] The higher FEs for $HCOO^-$ observed with the MEA-type configuration compared to H-cell studies suggest that a very high local pH at the reaction interface might favor the reduction of CO_2 to $HCOO^-$ at the expense of CO production, particularly at the high cathodic overpotentials needed to achieve high current densities. This observation is consistent with the remarkably high FE toward $HCOO^-$ over Ag GDEs under

extremely alkaline conditions (i.e., up to 38% with a 10 M KOH catholyte) reported by the Sargent and Sinton group.[21] Nevertheless, we note that modeling studies of Ag GDEs show that, under buffered conditions, a very large change of local pH occurs between 0 and 50 mA cm^{-2} (up to a pH of ca. 12) while variations thereafter are modest.[11] Taking this into account, the increasing FE for $HCOO^-$ we observe with total current density is likely driven by higher cathodic overpotentials (once the electrode is operating at pH $\geq$ 12) rather than by further changes of local pH. Furthermore, as in previous studies,[21,38] our results indicate that most of the $HCOO^-$ formed over the Ag cathode was transported across the AEM and readily oxidized to CO_2 over the IrO_2 anode. This is evidenced by (a) the post-reaction concentration of $HCOO^-$ in the anolyte, which is much lower than it would be in the absence of decomposition (**Table S1**), and by (b) the increasing fraction of the anodic current (at $j_{total} \geq 250$ mA cm^{-2}) that could not be attributed to the oxygen evolution reaction (OER) (**Figure 2C**). Although corrosion of the carbon paper substrate of the IrO_2/C anode would likely compromise the performance of the device under long-term operation, control experiments with an argon-fed cell revealed that the carbon-based anode is only negligibly oxidized over the short time scales studied in this work, even at very high cell voltages (**Figure S2**). Furthermore, water oxidation to hydrogen peroxide—another possible anodic reaction—is very strongly suppressed over IrO_2.[39,40] In contrast, the oxidation of formic acid (likely formed in the buffered anolyte from cathodically-generated $HCOO^-$ transported across the AEM) has facile kinetics over IrO_2 electrodes and competes directly with the OER, as reported by Comninellis and co-workers.[41,42] We confirmed that $HCOO^-$ is significantly oxidized by the IrO_2/C anode (i.e., FE ca. 20% at 200 mA cm^{-2}) even when it is extrinsically added to the 0.1 M $KHCO_3$ anolyte (**Figure S4** and the explanation therein), even though in this scenario this reaction is hindered by $HCOO^-$ having to diffuse

through the thick GDL of the anode to reach the IrO_2 catalyst (a limitation that is absent when $HCOO^-$ is transported across the membrane). In this context, CO_2 reduction to $HCOO^-$ with AEM-based MEAs is particularly undesirable, because energy is spent to generate (and then decompose) a product that cannot be recovered. This observation motivates further research on the factors that result in higher $HCOO^-$ FEs than those typically observed in H-cells, and on devising strategies to limit this side reaction.

3.3. Analysis of mass flows and CO_2 crossover through the membrane. Under basic and neutral conditions (i.e., with H_2O as the proton donor), the eCO_2RR and the HER generate OH^- anions at the cathode (equations 1-3) that react with CO_2 to generate bicarbonate and carbonate anions (equations 4 and 5). The transport of these species as charge carriers through the AEM results in the undesired crossover of CO_2 from the cathodic to the anodic compartment of the device.

Release of OH^- at the cathode

$$CO_2 + 2\ e^- + H_2O \rightarrow CO + 2\ OH^- \quad (1)$$

$$CO_2 + 2\ e^- + H_2O \rightarrow HCOO^- + OH^- \quad (2)$$

$$2\ H_2O + 2\ e^- \rightarrow H_2 + 2\ OH^- \quad (3)$$

Neutralization of CO_2 at the cathode

$$CO_2 + OH^- \leftrightarrow HCO_3^- \quad (4)$$

$$HCO_3^- + OH^- \leftrightarrow CO_3^{2-} + H_2O \quad (5)$$

Gas evolution (O_2 and CO_2) at the anode

$$2\ H_2O \rightarrow O_2 + 4\ H^+ + 4\ e^- \quad (6)$$

$$HCO_3^- + H^+ \rightarrow CO_2 + H_2O \quad (7)$$

$$CO_3^{2-} + 2\ H^+ \rightarrow CO_2 + H_2O \quad (8)$$

$$HCOOH \rightarrow CO_2 + 2\,H^+ + 2\,e^- \quad (9)$$

CO_2 crossover will tend to change the molar flow rate coming out of the cathodic compartment in a way that is not necessarily predictable from the reaction stoichiometry. **Figure 3A** shows the molar flow rate measured at the cathodic outlet at different current densities. In principle, the total molar flow rate should be conserved when CO_2 is reduced to CO, but we observed a decrease of the flow of up to ca. 10% in the region of high CO selectivity (50-250 mA cm^{-2}). Conversely, at current densities above 250 mA cm^{-2}, the flow rate tended to increase due to the addition of a component (hydrogen) to the gas phase from a reagent in the liquid phase (water). Gas flows from the anode were significantly higher than expected from oxygen evolution alone, and the decrease of the cathodic outlet flow was accompanied by the detection of an increasing amount of CO_2 at the outlet of the anodic compartment up until the onset of hydrogen evolution (**Figure 3B**). This result evidenced the transport through the AEM of charged species originating from cathodic CO_2 (i.e., HCO_3^-, CO_3^{2-} and $HCOO^-$) and their subsequent release as CO_2 over the anode (equations 6-9). It is interesting to note that both CO_2 crossover and total CO_2 consumption (**Figures 3C** and **4A**, respectively) plateau at high current densities, which suggests the occurrence of mass transfer limitations and the depletion of CO_2 at the reaction interface. **Figure 3C** shows that most of the CO_2 crossover originates from CO_2 neutralization to HCO_3^- or CO_3^{2-}, although a substantial fraction of CO_2 is "lost" to the anode as $HCOO^-$, particularly when $j_{total} \geq 250$ mA cm^{-2}. As argued previously, the oxidation of the carbon substrate of the anode contributes very negligibly to the CO_2 detected in the anodic compartment (**Figure S2**), and the total mass balance of carbon (i.e., practically 100% for all current densities) further supports this observation (**Figure 3C**).

We remark that neglecting the variation of the molar flow rate at the outlet of the cathode can result in an overestimation of the reaction rate of CO_2 reduction to CO and thus in an erroneous assessment of the performance of the device. For example, using the estimated flow rate at the outlet instead of the actual (**Figure 3A**) leads to calculating a maximum j_{CO} that is ca. 6% higher than the actual value. Lowering the flow rate of CO_2 fed into the cathode (e.g., to achieve a higher single-pass conversion) accentuated this issue because the decrease of the flow was proportionally larger (**Figure S5**). Because it results in higher cumulative Faradaic efficiency for gas-phase products, this miscalculation can lead to underestimating the production of liquid-phase products, particularly if they can be transported across the membrane and oxidized over the anode, such as $HCOO^-$. Furthermore, using a highly alkaline electrolyte in the cathodic compartment could possibly aggravate this problem due to the neutralization of CO_2 by the electrolyte itself in addition to that by reaction-generated OH^- ions.[20,21] These observations underscore the importance of measuring the actual molar outlet flow from the cathode when characterizing the performance of CO_2 reduction devices operating at high current densities in order to avoid overstated claims of efficiency and selectivity.

Lastly, comparing the amount of CO_2 (excluding the CO_2 released from formic acid oxidation) and O_2 evolved over the anode provided an indication of the main charge carrier across the AEM (**Figure 3D**). For example, if all the charge is carried by OH^-, CO_3^{2-} or HCO_3^-, the CO_2/O_2 ratios at the anode would be 0, 2 or 4, respectively.[30] We note that the accuracy of this calculation is improved when anodic CO_2 originating from $HCOO^-$ oxidation is excluded; therefore, the numerator of the ratio corresponds only to CO_2 that crosses over as HCO_3^-/CO_3^{2-} (i.e., the upper curve in **Figure 3C**). Below 250 mA cm^{-2} this ratio is practically constant and equal to ca. 2, indicating that CO_3^{2-} (and not HCO_3^-) is the main charge carrier across the AEM

in the absence of hydrogen evolution. However, upon the onset of the HER there is a rapid decrease of the anodic CO_2/O_2 ratio, which is most likely a consequence of increased transport across the membrane of OH- produced in the HER. We remark that these results provide experimental validation to the modeling efforts of Weber et al.,[22] who predicted that the main charge-carrying species would be carbonate anions in AEM-based MEAs.

While a technoeconomic analysis is beyond the scope of this work, it is clear that CO_2 crossover imposes a significant economic penalty on AEM-based eCO_2RR devices, considering that the price of CO_2 would be linked to the (currently elevated) costs of carbon capture schemes.[43] Even though our electrolyzer achieves outstanding figures of merit in terms of selectivity, current density and cell voltage, **Figure 4B** shows that, overall, CO_2 utilization is rather poor: even at low total current densities, less than half of the CO_2 consumed by the device (which is shown in **Figure 4A**) is due to its conversion to the target product. In contrast to previous modeling results,[22] CO_2 utilization worsens with increasing current density, and at the point of the highest rate of CO production (i.e., at 250 mA cm^{-2}), close to 60% of the CO_2 consumed is not actually converted to CO. These results illustrate some of the tradeoffs that have to be considered for the development of MEA-based eCO_2RR devices, and encourage the consideration of reactant utilization as a valuable metric to complement the evaluation of CO_2 reduction electrolyzers operating at high current densities. In this regard, we note that many different factors (e.g., membrane chemistry, electrolyte composition, mass transfer at the interface) are expected to have an influence on CO_2 crossover.[44] Consequently, future studies aimed at investigating these aspects are required to tailor the electrode-membrane interface and mitigate this phenomenon.[27] Furthermore, future technoeconomic analyses will be valuable to assess the consequences of CO_2 crossover and to establish design parameters, and we highlight

the fact that there is also great potential in investigating process-level solutions (e.g., outlet recirculation, integration with a different anodic reaction) to improve reactant utilization in eCO_2RR devices.

4. CONCLUSIONS

In this work, we demonstrated the potential of porous Ag membranes to act as effective gas diffusion electrodes for CO_2 reduction to CO at high current densities. By using the Ag membranes as gas-fed cathodes (humidified CO_2) in tandem with a liquid-fed IrO_2/C anode (0.1 M $KHCO_3$) in a membrane-electrode assembly with a Sustainion AEM, a maximum partial current density for CO of ca. 200 mA cm^{-2} at a cell voltage of ca. 3.3 V was achieved. Hydrogen evolution was effectively suppressed up to total current density of 250 mA cm^{-2}; but operating the cell beyond this point resulted in a rapid increase of H_2 production coupled with the collapse of eCO_2RR activity. Furthermore, we showed large losses of CO_2 to the anode compartment of the cell due to transport of $HCOO^-$ and of HCO_3^-/ CO_3^{2-}—generated from CO_2 reduction and neutralization, respectively—across the anion-exchange membrane, and CO_3^{2-} was found to be the main charge-carrying species across the AEM. Failure to account for the decrease of the flow rate at the cathodic outlet caused by the non-stoichiometric neutralization and transport of CO_2 to the anode can lead to overstated claims of device performance. Even though the exchange-MEA configuration achieved outstanding results in terms of activity and selectivity, overall CO_2 utilization in the AEM-based MEA-type electrolyzer is poor, with less than half of the consumed CO_2 going toward the production of the target product. These results call for the adoption of CO_2 utilization as complementary criterion for the evaluation of devices operating at industrially relevant current densities, and encourages further research into strategies to mitigate CO_2

crossover while retaining the favorable features (i.e., high selectivity and low ohmic losses) of AEM-based membrane-electrode assemblies in CO_2 reduction.

ASSOCIATED CONTENT

Supporting Information. Multivariable calibration procedure of the mass flow meter. Calculation of the Faradaic efficiencies and partial current densities. HPLC analysis of liquid products. Calculation of CO_2 crossover. XPS analysis of a porous Ag electrode. Products and outlet flows with argon as inlet gas. Cell voltage and gas-phase selectivity versus time in a typical galvanostatic electrolysis. Cathodic outlet flow rates for different inlet flow rates.

AUTHOR INFORMATION

Corresponding Author

*Address: Surface Physics & Catalysis (SurfCat) section, Department of Physics, Technical University of Denmark, Fysikvej Bld. 312, 2800 Kgs. Lyngby, Denmark. Phone +45 45 25 33 44. E-mail: brse@fysik.dtu.dk.

Author Contributions

G.O.L., P.S-H. and J.P.H. and K.Z. developed the experimental setup and carried out measurements. G.O.L. performed the data analysis, and wrote the manuscript with input from all co-authors. K.T.T., I.C. and B.S. conceived the project and oversaw its development.

ACKNOWLEDGMENTS

This work was supported by the Villum Foundation V-SUSTAIN grant 9455 to the Villum Center for the Science of Sustainable Fuels and Chemicals. The authors acknowledge the DTU Center for Electron Nanoscopy for access to their facilities, and thank Ming Ma, Sebastian Dalsgaard and Ezra L. Clark for the valuable discussions.

REFERENCES

(1) Kondratenko, E. V.; Mul, G.; Baltrusaitis, J.; Larrazábal, G. O.; Pérez-Ramírez, J. Status and Perspectives of CO_2 Conversion into Fuels and Chemicals by Catalytic, Photocatalytic and Electrocatalytic Processes. *Energy Environ. Sci.* **2013**, *6*, 3112–3135.

(2) Chen, A.; Lin, B. L. A Simple Framework for Quantifying Electrochemical CO_2 Fixation. *Joule* **2018**, *2*, 594–606.

(3) Bushuyev, O. S.; De Luna, P.; Dinh, C. T.; Tao, L.; Saur, G.; van de Lagemaat, J.; Kelley, S. O.; Sargent, E. H. What Should We Make with CO_2 and How Can We Make It? *Joule* **2018**, *2*, 825–832.

(4) Nitopi, S. A.; Bertheussen, E.; Scott, S. B.; Liu, X.; Albert, K.; Horch, S.; Seger, B.; Stephens, I. E. L.; Chan, K.; Nørskov, J. K.; Jaramillo, T.F.; Chorkendorff, I. Progress and Perspectives of Electrochemical CO_2 Reduction on Copper in Aqueous Electrolyte. *Chem. Rev.* **2019**, *119*, 7610–7672.

(5) Liu, X.; Xiao, J.; Peng, H.; Hong, X.; Chan, K.; Nørskov, J. K. Understanding Trends in Electrochemical Carbon Dioxide Reduction Rates. *Nat. Commun.* **2017**, *8:15438*, 1–7.

(6) Rosen, J.; Hutchings, G. S.; Lu, Q.; Rivera, S.; Zhou, Y.; Vlachos, D. G.; Jiao, F. Mechanistic Insights into the Electrochemical Reduction of CO_2 to CO on Nanostructured

Ag Surfaces. *ACS Catal.* **2015**, *5*, 4293–4299.

(7) Larrazábal, G. O.; Martín, A. J.; Pérez-Ramírez, J. Building Blocks for High Performance in Electrocatalytic CO_2 Reduction: Materials, Optimization Strategies, and Device Engineering. *J. Phys. Chem. Lett.* **2017**, *8*, 3933–3944.

(8) Verma, S.; Kim, B.; Jhong, H. R. M.; Ma, S.; Kenis, P. J. A. A Gross-Margin Model for Defining Technoeconomic Benchmarks in the Electroreduction of CO_2. *ChemSusChem* **2016**, *9*, 1972–1979.

(9) Jouny, M.; Luc, W.; Jiao, F. General Techno-Economic Analysis of CO_2 Electrolysis Systems. *Ind. Eng. Chem. Res.* **2018**, *57*, 2165–2177.

(10) Higgins, D.; Hahn, C.; Xiang, C.; Jaramillo, T. F.; Weber, A. Z. Gas-Diffusion Electrodes for Carbon Dioxide Reduction: A New Paradigm. *ACS Energy Lett.* **2019**, *4*, 317–324.

(11) Burdyny, T.; Smith, W. A. CO_2 Reduction on Gas-Diffusion Electrodes and Why Catalytic Performance Must Be Assessed at Commercially-Relevant Conditions. *Energy Environ. Sci.* **2019**, *12*, 1442–1453.

(12) Hori, Y.; Kikuchi, K.; Suzuki, S. Production of CO and CH_4 in Electrochemical Reduction of CO_2 at Metal Electrodes in Aqueous Hydrogencarbonate Solution. *Chem. Lett.* **1985**, 1695–1698.

(13) Hatsukade, T.; Kuhl, K. P.; Cave, E. R.; Abram, D. N.; Jaramillo, T. F. Insights into the Electrocatalytic Reduction of CO_2 on Metallic Silver Surfaces. *Phys. Chem. Chem. Phys.* **2014**, *16*, 13814–13819.

(14) Zhao, S.; Jin, R.; Jin, R. Opportunities and Challenges in CO2 Reduction by Gold- and

Silver-Based Electrocatalysts: From Bulk Metals to Nanoparticles and Atomically Precise Nanoclusters. *ACS Energy Lett.* **2018**, *3*, 452–462.

(15) Bidault, F.; Kucernak, A. A Novel Cathode for Alkaline Fuel Cells Based on a Porous Silver Membrane. *J. Power Sources* **2010**, *195*, 2549–2556.

(16) Kucernak, A.; Bidault, F.; Smith, G. Membrane Electrode Assemblies Based on Porous Silver Electrodes for Alkaline Anion Exchange Membrane Fuel Cells. *Electrochim. Acta* **2012**, *82*, 284–290.

(17) Dinh, C.-T.; Burdyny, T.; Kibria, M. G.; Seifitokaldani, A.; Gabardo, C. M.; Pelayo García de Arquer, F.; Kani, A.; Edwards, J. P.; De Luna, P.; Bushuyev, O. S.; Zhou, C.; Quintero-Bermudez, R.; Pang, Y.; Sinton, D.; Sargent, E.H. CO_2 Electroreduction to Ethylene via Hydroxide-Mediated Copper Catalysis at an Abrupt Interface. *Science.* **2018**, *360*, 783–787.

(18) Cifrain, M.; Kordesch, K. V. Advances, Aging Mechanism and Lifetime in AFCs with Circulating Electrolytes. *J. Power Sources* **2004**, *127*, 234–242.

(19) Martín, A. J.; Larrazábal, G. O.; Pérez-Ramírez, J. Towards Sustainable Fuels and Chemicals Through the Electrochemical Reduction of CO_2: Lessons from Water Electrolysis. *Green Chem.* **2015**, *17*, 5114–5130.

(20) Dinh, C. T.; García De Arquer, F. P.; Sinton, D.; Sargent, E. H. High Rate, Selective, and Stable Electroreduction of CO_2 to CO in Basic and Neutral Media. *ACS Energy Lett.* **2018**, *3*, 2835–2840.

(21) Gabardo, C. M.; Seifitokaldani, A.; Edwards, J. P.; Dinh, C. T.; Burdyny, T.; Kibria, M.

G.; O'Brien, C. P.; Sargent, E. H.; Sinton, D. Combined High Alkalinity and Pressurization Enable Efficient CO_2 Electroreduction to CO. *Energy Environ. Sci.* **2018**, *11*, 2531–2539.

(22) Weng, L.-C.; Bell, A. T.; Weber, A. Z. Towards Membrane-Electrode Assembly Systems for CO2 Reduction: A Modeling Study. *Energy Environ. Sci.* **2019**, 1950–1968.

(23) Delacourt, C.; Ridgway, P. L.; Kerr, J. B.; Newman, J. Design of an Electrochemical Cell Making Syngas ($CO+H_2$) from CO_2 and H_2O Reduction at Room Temperature. *J. Electrochem. Soc.* **2007**, *155*, B42.

(24) Hori, Y.; Ito, H.; Okano, K.; Nagasu, K.; Sato, S. Silver-Coated Ion Exchange Membrane Electrode Applied to Electrochemical Reduction of Carbon Dioxide. *Electrochim. Acta* **2003**, *48*, 2651–2657.

(25) Li, Y. C.; Zhou, D.; Yan, Z.; Gonçalves, R. H.; Salvatore, D. A.; Berlinguette, C. P.; Mallouk, T. E. Electrolysis of CO_2 to Syngas in Bipolar Membrane-Based Electrochemical Cells. *ACS Energy Lett.* **2016**, *1*, 1149–1153.

(26) Salvatore, D. A.; Weekes, D. M.; He, J.; Dettelbach, K. E.; Li, Y. C.; Mallouk, T. E.; Berlinguette, C. P. Electrolysis of Gaseous CO_2 to CO in a Flow Cell with a Bipolar Membrane. *ACS Energy Lett.* **2018**, *3*, 149–154.

(27) Pătru, A.; Binninger, T.; Pribyl, B.; Schmidt, T. J. Design Principles of Bipolar Electrochemical Co-Electrolysis Cells for Efficient Reduction of Carbon Dioxide from Gas Phase at Low Temperature. *J. Electrochem. Soc.* **2019**, *166*, F34–F43.

(28) Kutz, R. B.; Chen, Q.; Yang, H.; Sajjad, S. D.; Liu, Z.; Masel, R. I. Sustainion

Imidazolium-Functionalized Polymers for Carbon Dioxide Electrolysis. *Energy Technol.* **2017**, *5*, 929–936.

(29) Yang, H.; Kaczur, J. J.; Sajjad, S. D.; Masel, R. I. Electrochemical Conversion of CO_2 to Formic Acid Utilizing Sustainion™ Membranes. *J. CO2 Util.* **2017**, *20*, 208–217.

(30) Liu, Z.; Yang, H.; Kutz, R.; Masel, R. I. CO_2 Electrolysis to CO and O_2 at High Selectivity, Stability and Efficiency Using Sustainion Membranes. *J. Electrochem. Soc.* **2018**, *165*, J3371–J3377.

(31) Endrődi, B.; Kecsenovity, E.; Samu, A.; Darvas, F.; Jones, R. V.; Török, V.; Danyi, A.; Janáky, C. Multilayer Electrolyzer Stack Converts Carbon Dioxide to Gas Products at High Pressure with High Efficiency. *ACS Energy Lett.* **2019**, *4*, 1770–1777.

(32) Kaczur, J. J.; Yang, H.; Liu, Z.; Sajjad, S. D.; Masel, R. I. Carbon Dioxide and Water Electrolysis Using New Alkaline Stable Anion Membranes. *Front. Chem.* **2018**, *6*, 1–16.

(33) Lin, M.; Han, L.; Singh, M. R.; Xiang, C. An Experimental- and Simulation-Based Evaluation on the CO_2 Utilization Efficiency in Aqueous-Based Electrochemical CO_2 Reduction Reactors with Ion-Selective Membranes. *ACS Appl. Energy Mater.* **2019**, *2*, 5843–5850.

(34) Sterlitech Corporation. Silver Membrane Filters. Available online at https://www.sterlitech.com/media/wysiwyg/datasheet/Silver_Membrane_Data_Sheet.pdf (Accessed June 2019).

(35) Larrazábal, G. O.; Martín, A. J.; Mitchell, S.; Hauert, R.; Pérez-Ramírez, J. Synergistic Effects in Silver–Indium Electrocatalysts for Carbon Dioxide Reduction. *J. Catal.* **2016**,

343, 266–277.

(36) Hoshi, N.; Kato, M.; Hori, Y. Electrochemical Reduction of CO_2 on Single Crystal Electrodes of Silver Ag(111), Ag(100) and Ag(100). *J. Electroanal. Chem.* **1997**, *440*, 283–286.

(37) Clark, E. L.; Ringe, S.; Tang, M.; Walton, A.; Hahn, C.; Jaramillo, T. F.; Chan, K.; Bell, A. T. Influence of Atomic Surface Structure on the Activity of Ag for the Electrochemical Reduction of CO_2 to CO. *ACS Catal.* **2019**, *9*, 4006–4014.

(38) Li, Y. C.; Yan, Z.; Hitt, J.; Wycisk, R.; Pintauro, P. N.; Mallouk, T. E. Bipolar Membranes Inhibit Product Crossover in CO_2 Electrolysis Cells. *Adv. Sustain. Syst.* **2018**, *2*, 1700187.

(39) Siahrostami, S.; Li, G. L.; Viswanathan, V.; Nørskov, J. K. One- or Two-Electron Water Oxidation, Hydroxyl Radical, or H_2O_2 Evolution. *J. Phys. Chem. Lett.* **2017**, *8*, 1157–1160.

(40) Yang, S.; Verdaguer-Casadevall, A.; Arnarson, L.; Silvioli, L.; Čolić, V.; Frydendal, R.; Rossmeisl, J.; Chorkendorff, I.; Stephens, I. E. L. Toward the Decentralized Electrochemical Production of H_2O_2: A Focus on the Catalysis. *ACS Catal.* **2018**, *8*, 4064–4081.

(41) Fierro, S.; Nagel, T.; Baltruschat, H.; Comninellis, C. Investigation of Formic Acid Oxidation on Ti/IrO_2 Electrodes Using Isotope Labeling and Online Mass Spectrometry. *Electrochem. Solid-State Lett.* **2008**, *11*, E20.

(42) Fierro, S.; Ouattara, L.; Calderon, E. H.; Passas-Lagos, E.; Baltruschat, H.; Comninellis,

C. Investigation of Formic Acid Oxidation on Ti/IrO2 Electrodes. *Electrochim. Acta* **2009**, *54*, 2053–2061.

(43) Keith, D. W.; Holmes, G.; St. Angelo, D.; Heidel, K. A Process for Capturing CO_2 from the Atmosphere. *Joule* **2018**, *2*, 1573–1594.

(44) Ziv, N.; Mustain, W. E.; Dekel, D. R. The Effect of Ambient Carbon Dioxide on Anion-Exchange Membrane Fuel Cells. *ChemSusChem* **2018**, *11*, 1136–1150.

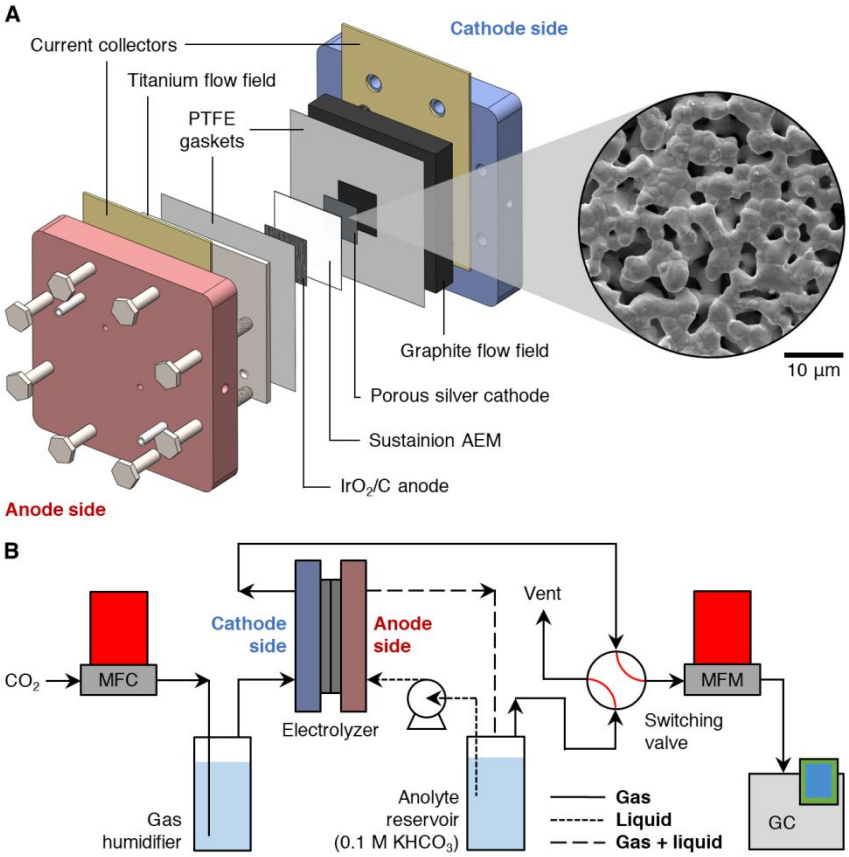

Figure 1. (A) MEA-type electrolytic cell for CO_2 reduction with a gas-fed cathode and a liquid-fed anode. (B) Flow diagram of the electrolysis setup. An automatic switching valve enabled the staggered measurement of the molar flow rate using a mass flow meter (MFM), in tandem with their compositional analysis via GC. A droplet condenser (not shown) was placed downstream of the cathode compartment.

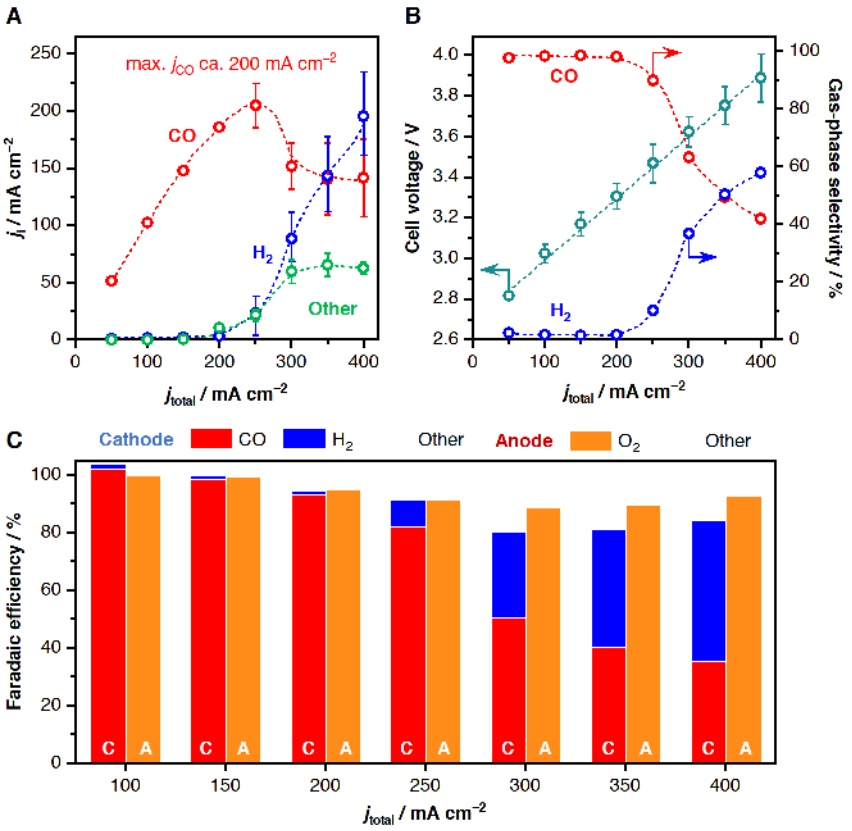

Figure 2. (A) Partial current densities (j_i) for different products as a function of the total current density (j_{total}) over a porous Ag cathode integrated into a MEA with a Sustainion AEM and an IrO_2/C anode. The error bars represent the standard error (SE) of the mean of 4 independent measurements. Error bars smaller than the symbol size are omitted for clarity. Trendlines are provided as a visual aid. (B) Cell voltage and gas-phase selectivity, defined as j_i / ($j_{CO} + j_{H2}$), as a function of the total current density. Operating the electrolyzer at current densities higher than 250 mA cm^{-2} resulted in periodic oscillations likely associated with mass transfer limitations. (C) Faradaic efficiencies over the porous Ag cathode (indicated by C) and the IrO_2/C anode (indicated by A). The values shown correspond to the mean FEs of 4 independent experiments. The fractions of the current that do not correspond to gas-phase products (indicated as "Others") are most likely attributable to $HCOO^-$ formation and decomposition, respectively.

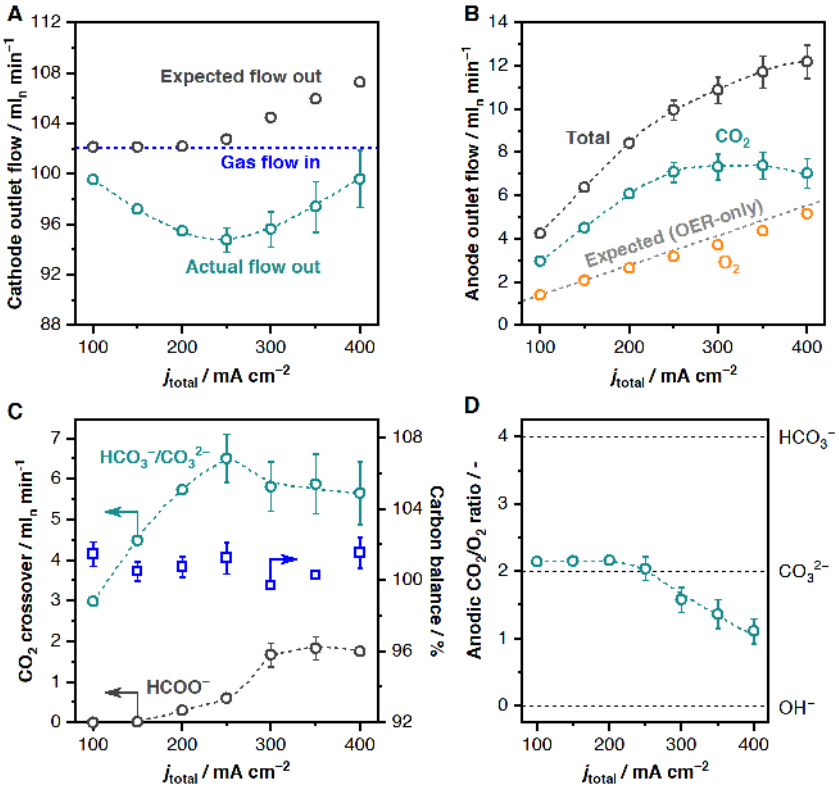

Figure 3. (A) Actual and expected outlet gas flows from the cathodic compartment of the electrolyzer as a function of the total current density (j_{total}). The inlet CO_2 flow (indicated by the horizontal dashed line) was 102.06 ± 0.07 ml_n min^{-1}. The expected outlet flow was calculated from the data in **Figure 2C** based on the FEs for the gas-phase products and the reaction stoichiometry. (B) Total and per-component gas flows evolved over the anode as a function of j_{total}. The expected anodic outlet flow in the absence of CO_2 crossover (dashed line) corresponds to a 100% FE for the OER. (C) CO_2 crossover through the AEM as different anionic species as a function of j_{total} and total mass balance of carbon around the cell. (D) Ratio of CO_2 to O_2 evolved over the anode as a function of j_{total}. The dashed lines indicate the theoretical values of CO_2/O_2 if all the current were carried by a single anionic species.

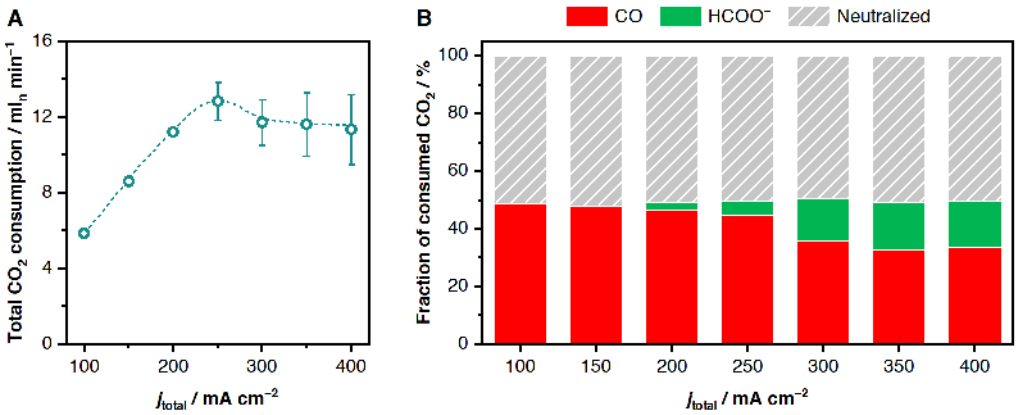

Figure 4. (A) Total consumption of CO_2 in the electrolyzer as a function of the total current density. The plateau that occurs at $j_{total} \geq 250$ mA cm^{-2} is indicative of mass transfer-limited operation. (B) Breakdown of CO_2 consumed at different total current densities (j_{total}) due to (1) CO evolution, and lost to the anode through (2) $HCOO^-$ evolution and (3) neutralization to HCO_3^-/CO_3^{2-}. The results highlight the overall poor utilization of consumed CO_2 in the AEM-based MEA-type electrolyzer.

Table of Contents Graphic